ICARUS 112, 187–203 (1994)

Merging Magellan Emissivity and SAR Data for Analysis of Venus Surface Dielectric Properties

BRUCE A. CAMPBELL

Center for Earth and Planetary Studies, National Air and Space Museum, Washington, DC 20560
E-mail: campbell@ceps.nasm.edu

Received March 25, 1994; revised August 23, 1994

Integration of Magellan datasets for Venus is an important part of characterizing the geology of the surface. We analyze the global average behavior of radar backscatter and emissivity and find that for incidence angles greater than 30° the two parameters can be modeled by the behavior of a single-dielectric surface ($\varepsilon \sim 4.15$) with variable roughness. Based on this result, we propose a model which relates the HH backscatter and H-polarized emissivity to values for a relative roughness fraction and dielectric constant. Maps of the model solutions are presented for the region 34°S–54°N. Removal of the contribution of roughness to the emissivity permits rapid identification of regions with anomalous composition or density. In smooth areas, the model typically yields dielectric constant values in good agreement with those calculated from the altimeter-derived reflectivities, but it appears that the model is more reliable than the Hagfors results for rough surfaces. The permittivity in highland regions rises with altitude, and the data for these areas are more consistent with a single high-dielectric interface (single and multiple scattering) than with internal volume scattering. Higher dielectric constants are associated with both smooth and rough terrains, but the general tendency is toward greater roughness with higher permittivity. This may suggest that a mechanical weathering process occurs in the formation of high-dielectric mineral phases. There are variations in dielectric constant within lava flow complexes (up to values of 9), which may reflect differences in the chemical content of the rock. Three major types of mantling deposits are identified: (1) high-permittivity ($\varepsilon = 7–8$) units associated with parabolic crater features and interpreted to be fine-grained material with a high proportion of metallic phases; (2) low-permittivity ($\varepsilon = 2–3$) crater-related splotches or haloes, interpreted to be fine-grained material with minimal or weathered metallic minerals; (3) low-permittivity deposits with no associated crater, tentatively attributed to soil or pyroclastic/ignimbrite eruptions. Within each type of deposit there is a range of surface roughness and radar backscatter strength, which are related to the original surface roughness and the depth of the mantling material.

INTRODUCTION

Data obtained by earth-based and orbital radar systems are nearly the only source of information on the surface properties of Venus, so interpretation of these measurements is a significant issue in completing a geologic reconnaisance of the planet. To fully characterize the surface, it is necessary to incorporate all available microwave datasets to define roughness and dielectric constant variations. In general, the effects of roughness and dielectric changes will vary with viewing geometry and the type of observation (backscatter versus emission), so deconvolving their relative contributions to any one measurement is often difficult. In terrestrial radar geology applications the importance of dielectric variations is rarely addressed due to the unknown water content and porosity of the target materials. For Venus, the lack of moisture at the surface and the acquisition of complementary backscatter, emissivity, and reflectivity (from near-nadir backscatter) datasets may permit a rigorous separation of roughness and dielectric effects.

The Magellan spacecraft used its high-gain antenna to measure radar backscatter and passive microwave emission from Venus' surface. These observations are interleaved in time so that each backscatter value is accompanied by an emissivity measurement for the same antenna footprint (Pettengill *et al.* 1992). Similar measurements were carried out with the Pioneer–Venus spacecraft, and both datasets have shown that the surface materials vary widely in their emissivity, with the lowest values found in regions above a radius of ~6053 km (Pettengill *et al.* 1988, 1992). While the very low emissivity areas are of limited spatial extent, interpreting the SAR (synthetic aperture radar) and emissivity data for regions below this elevation is still complicated by the differing influence of roughness and dielectric constant on the two parameters. A third dataset was collected by the Magellan altimeter system, which measures backscatter within 15° of the nadir. These radar echoes were modeled using the Hagfors expression for gently undulating surface returns to estimate large-scale rms slope and Fresnel reflectivity (Ford and Pettengill 1992). These values are expected

0019-1035/94 $6.00

to be quite accurate in smooth regions, but require a correction for diffuse scattering from rough terrain which is difficult to validate (Pettengill *et al.* 1988).

Several authors have investigated the dielectric properties of geologic features on Venus. The interpretation of the very low emissivity areas in the highlands is still under discussion, but it seems likely that the mechanism is either loading of the rocks with conductive minerals or volume scattering within a nearly transparent matrix of soil (Pettengill *et al.* 1988, 1992; Tryka and Muhleman 1992; Wilt 1992; Shepard *et al.* 1994). Klose *et al.* (1992) suggested that pyrite is the loading mineral based on phase equilibrium studies of various materials under Venus conditions, while Burns and Straub (1993) and Fegley *et al.* (1992) feel that several other minerals may be more likely candidates. Shepard *et al.* (1994) propose that the low emissivities are due to ferroelectric minerals, whose dielectric properties change with temperature. Tryka and Muhleman (1992) show that volume scattering from reflective objects in a low-loss matrix could be responsible for the observed properties of Alpha Regio, but Wilt (1992) disputes their findings with regard to the efficiency of the process in lowering the emissivity. Campbell *et al.* (1992), in their study of extended crater deposits, inferred that dark parabolic features near the craters Lind and Faustina have rather low dielectric constants (2.5–3.0), while Plaut and Arvidson (1992) found that one halo seen by Magellan and Goldstone has a smooth, high-dielectric surface. Areas of higher dielectric constant in the lowlands of Venus were also noted by Jurgens *et al.* (1988). Many of these lowland emissivity/reflectivity anomalies are associated with impact crater floors, flow features, or extended ejecta (Arvidson *et al.* 1992; Campbell *et al.* 1992; Schultz 1992). Robinson and Wood (1993) analyzed the emissivity for several volcanic edifices, and proposed that the presence of regions at high elevations which do not exhibit low emissivity are evidence for volcanism younger than the time scale required to concentrate the loading phase (or that this mineral does not exist in the lavas in these regions). They also suggest that low emissivities found around volcanic domes near these edifices represent alteration of the basalt by volcanic outgassing.

There is clearly a large amount of geochemical information to be gained from the Magellan emissivity data, but these measurements are also linked to the roughness of the surface. In this paper, a model is presented for the relationship between radar backscatter cross section and emissivity, based on observations of the mean global behavior of these parameters. This model relates the SAR and emissivity data to roughness and dielectric constant terms; the resulting maps allow rapid identification of areas with anomalous composition or density. The nature of surface scattering and emission, and the global correlation between these measurements, is discussed first. The model is then described, and maps of roughness and dielectric constant are presented for the area between 34°S and 54°N. The dielectric properties of several areas are discussed in detail, and some speculations are offered as to the nature of high- and low-permittivity materials found in various locales.

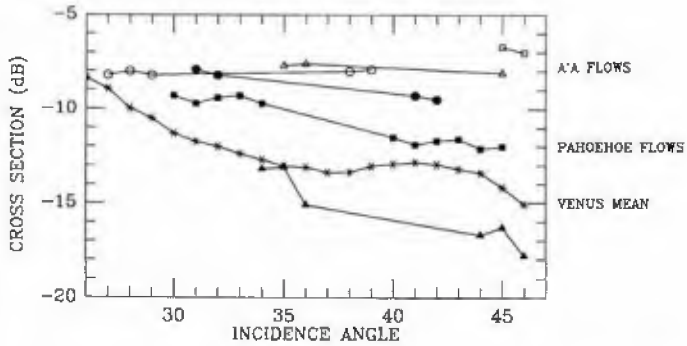

FIG. 1. Specific backscatter cross section versus incidence angle for six Hawaiian lava flows at interpolated *S*-band wavelength (12.6 cm). Data from Campbell and Campbell (1992). Rougher a'a flows are represented by open plot symbols, while smoother pahoehoe flows are shown by filled symbols. Note that the rougher flows have higher cross sections but shallow slopes, while smooth flows have low cross sections and steep slopes. Venus mean curve (asterisks) derived from global dataset of footprint-averaged SAR values. The upturn in the Venus mean values beyond 38° is likely due to the equatorial highlands imaged within this angular range (see Fig. 3).

SURFACE SCATTERING AND EMISSION

Radar backscatter is, in general, a function of both roughness at a variety of scales and the bulk dielectric properties of the target material. Roughness on scales that are large with respect to the wavelength can produce facet-like (quasi-specular) echoes, while roughness on scales close to that of the radar wavelength tends to produce "diffuse" returns. Figure 1 shows the effect of roughness on backscatter for six Hawaiian lava flows (see Campbell and Campbell 1992 for the derivation of these "*S*-band" echoes from AIRSAR data). The complex dielectric constant (permittivity) of the surface determines the reflectivity of any given element and the degree of attenuation experienced by radar energy passing through the material. To first order, the surface reflectivity can be expressed by the normal-incidence Fresnel reflection coefficient R_0,

$$R_0 = (\sqrt{\varepsilon} - 1)^2/(\sqrt{\varepsilon} + 1)^2, \quad (1)$$

where ε is the real part of the dielectric constant.

At 6- to 24-cm wavelengths, radar returns from terres-

trial lava flows appear to be largely single-scattered by surface roughness elements (Campbell *et al.* 1993). There is no evidence for significant volume scattering until the radar wavelength reaches 70 cm or more. If we assume that these same generalizations apply to Venus (imaged by Magellan at 12.6 cm wavelength), then changes in the dielectric constant will produce variations in backscatter proportional to the change in Fresnel reflectivity. Radar penetration and volume scattering are not likely to be important except in regions overlain by unconsolidated material.

Emissivity is defined as the ratio between the observed emitted radiation and that expected for a Planck blackbody at the same physical temperature (determined for Venus from a standard model of temperature lapse with elevation). The microwave emission from a surface is controlled in part by the dielectric constant, with higher values of directional hemispherical reflectivity leading to lower values of emissivity at the same viewing geometry. For a perfectly smooth surface, the emissivity E at emission angle ϕ and dielectric constant ε is given by the Fresnel transmission coefficients (Stratton 1947),

$$E_h = T_h = \frac{\sin 2\phi \sin 2\theta}{\sin^2(\theta + \phi)} \tag{2}$$

$$E_v = T_v = \frac{\sin 2\phi \sin 2\theta}{\sin^2(\theta + \phi)\cos^2(\phi - \theta)} \tag{3}$$

$$\theta = \sin^{-1}\left(\frac{\sin\phi}{\sqrt{\varepsilon}}\right) \tag{4}$$

where the h and v subscripts refer to horizontal and vertical polarization states, respectively.

In this paper, we assume that as the surface becomes rougher at the scale of the radar wavelength, the emissivity will move toward the average of the plane–surface transmission coefficients for the two polarizations. This is an approximation to a complicated relationship between roughness at different length scales and the emitted energy. Ulaby *et al.* (1987, p. 978) model the effect of varying large-scale (tens to hundreds of wavelengths) roughness on the emissivity. They show that for significant rms slopes (10° or more) values of E_h and E_v tend to pull toward the average of the plane–surface values with greater roughness. At very large rms slopes (20° or more), the absolute values of the emission curves also increase with roughness. For most areas on Venus other than ridge belts, corona rims, or other steep terrain, rms slopes tend to be lower than 10°, so the large-scale roughness effects modeled by Ulaby *et al.* will not play a significant role in the observed emissivity (Ford and Pettengill 1992). The effect of wavelength-scale roughness on emission has not been modeled (though it was considered by Hagfors (1970) and England (1975)), so we use the average of the plane–surface values for the two polarizations as an estimate of the rough-surface emissivity. A Lambertian surface will have equivalent E_h and E_v which are independent of emission angle, and the average emissivity used here is only slightly sensitive to this angle in the 20°–45° range relevant to Magellan observations. The calculated emissivity for various smooth and rough dielectric surfaces in H and V polarizations are shown in Fig. 2. Note that at lower dielectric constants or smaller values of ϕ the range of emissivity between smooth and rough surfaces decreases.

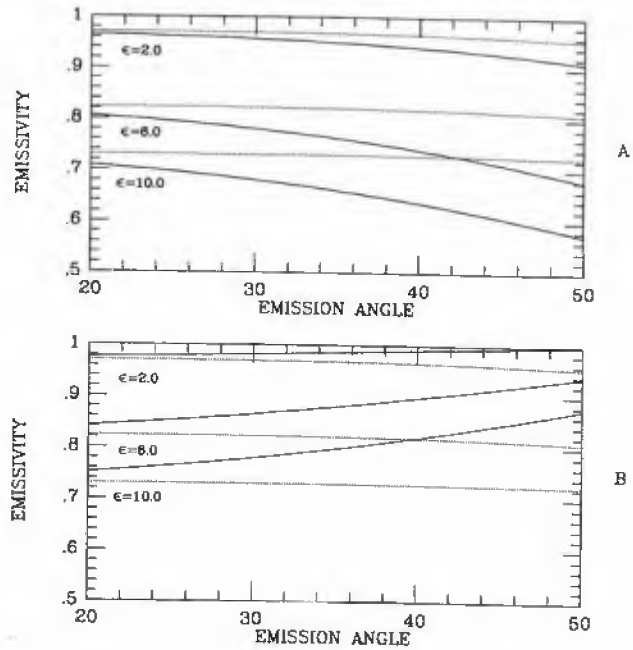

FIG. 2. Emissivity versus incidence angle for smooth and rough surfaces at varying dielectric constants. (A) Solid lines are the H-polarized emissivity for a smooth plane, while dotted lines are the average of H and V polarizations (a rough interface). (B) Solid lines are the V-polarized emissivity for a smooth plane, while dotted lines are the average of H and V polarizations. Note the increasing separation between smooth and rough terrain at higher dielectric constants.

In summary, the backscatter cross section of a surface seen at oblique incidence angles will increase with higher dielectric constant or greater roughness. H-polarized emissivity will decline with higher dielectric constants and increase with greater roughness, bounded by the values for smooth and rough surfaces. Incidence/emission angle has a strong effect on both measurements when the surface is smooth, but a minimal effect for rough terrain. Theoretical models for scattering and emission are not adequate to jointly predict these parameters over a large range of roughness; in order to deconvolve the relative roles of roughness and dielectric constant, we must derive an empirical relationship from observations made over large areas of the planet.

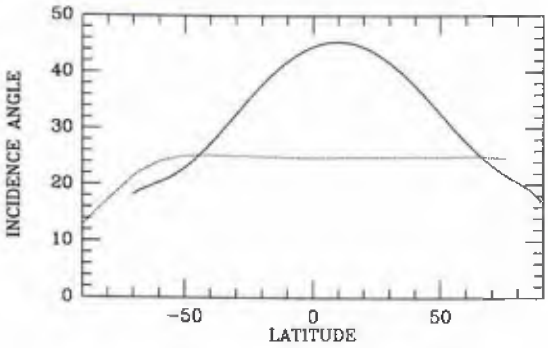

FIG. 3. Incidence angle versus latitude for Magellan left-looking (solid line) and right-looking (dotted line) profiles. Data from Saunders *et al.* (1992).

GLOBAL BEHAVIORS FROM MAGELLAN DATA

To study the global average behavior of radar backscatter and emissivity, we constructed a database of footprint locations (latitude, longitude), planetary radius, radar incidence angle, unfocused (footprint-averaged) HH SAR cross section (σ_0), and H-polarized emissivity from the Magellan ARCDR (Altimetry and Radiometry Composite Data Record) CD-roms. This database contains all footprints from Magellan orbits 361–3900 for which a useable pair of backscatter and emissivity measurements were obtained, for a total of approximately 6 million datapoints. As shown by Fig. 3, the incidence angle coverage of Magellan data is latitude dependent for the left-looking mode, and only the data collected in this nominal angular profile contain observations at angles greater than 25° (Saunders *et al.* 1992). If we restrict ourselves to angles greater than 30° (for reasons explained below), then our study area is limited to the latitude range from 34°S to 54°N. Despite this sampling bias, any given angular range contains a broad spectrum of surface units, and thus provides a view of the mean behavior of the surface at that angle.

Using these data files we can bin the emissivity and backscatter cross section values within a chosen range of incidence angles and elevations. Each specific backscatter cross section was calculated from the normalized values on the ARCDR by removing the Muhleman law correction (Saunders *et al.* 1992), and represents the average of the echoes over the antenna footprint. The planetary mean backscatter cross section as a function of incidence angle is shown on Fig. 1. Contour plots of emissivity versus backscatter cross section for all elevations on Venus are shown in Fig. 4, where we have split the incidence angle range into two bins (20–30°, >30°). In both plots there is an elongate region containing the majority of the surface points and a more sparsely populated region of higher σ_0, lower E values. Footprints in this lower "dogleg" are largely associated with areas above ~6053.0 km radius, as shown by Fig. 5, where we have limited the radius values to the lowlands.

It is clear that there is a linear relationship between emissivity and $\log(\sigma_0)$ for angles >30° and elevations less than ~6053.0 km. At lower values of the incident/emitted angle, there is no clear relationship between the two parameters. To better quantify the nature of the correlation, we averaged the emissivity as a function of backscatter cross section for three angle ranges (30–35°, 35–40°, and >40°). These average plots are shown in Fig. 6. Each graph displays a linear region and a rolloff toward lower values of emissivity at high σ_0. The low end of the plot and the location of the rolloff move toward higher σ_0 values at lower incidence angles.

The following explanations are offered for these observations.

1. The linear portions of the $E(\log \sigma_0)$ graphs for angles >30° represent the behavior of the "mean" Venus surface with increasing roughness. As shown above, both the backscatter cross section and the H-polarized emissivity are expected to rise with increasing roughness.

2. The poorer correlation between backscatter and emissivity at angles <30° is due to the breakdown of the simple relationship between wavelength-scale roughness and backscatter within this angular range. Hawaiian lava flows exhibit an ambiguity in HH backscatter power near 30° which often makes it impossible to discern pahoehoe from a'a textures (Fig. 1). This occurs because the quasi-specular component of the pahoehoe echoes rises more rapidly with decreasing incidence angle than does the diffuse return from the a'a, where the backscatter curves cross the relationship between brightness and roughness is lost.

3. The negative correlation between emissivity and σ_0 for bright areas above 6053.0 km represents the anomalous highland surfaces, whose elevated dielectric constants (or unique volume scattering geometry) enhance their reflectivity and lower their emissivity.

A check on our interpretations is provided by 11 orbits for which Magellan collected V-polarized emissivity data and VV SAR echoes. These orbits provide about 12,000 footprints on the surface with incidence angles >30°, and we have produced contour plots and mean emissivity versus σ_0 graphs as was done for the H-polarized data. The contour plot is shown in Fig. 7A, and the average H and V emissivity values (binned as a function of σ_0) are plotted in Fig. 7B. The V-polarized emissivity declines with greater σ_0 from an initial value of ~0.95 to converge with the average H-polarized data at about −9 dB. Although the absolute values of the E_v results have not been calibrated to the same degree as the E_h data (P. Ford, personal communication), these plots appear to support the use of the average of H- and V-polarized specular emissivities to estimate the emission from a rough surface (Fig. 2).

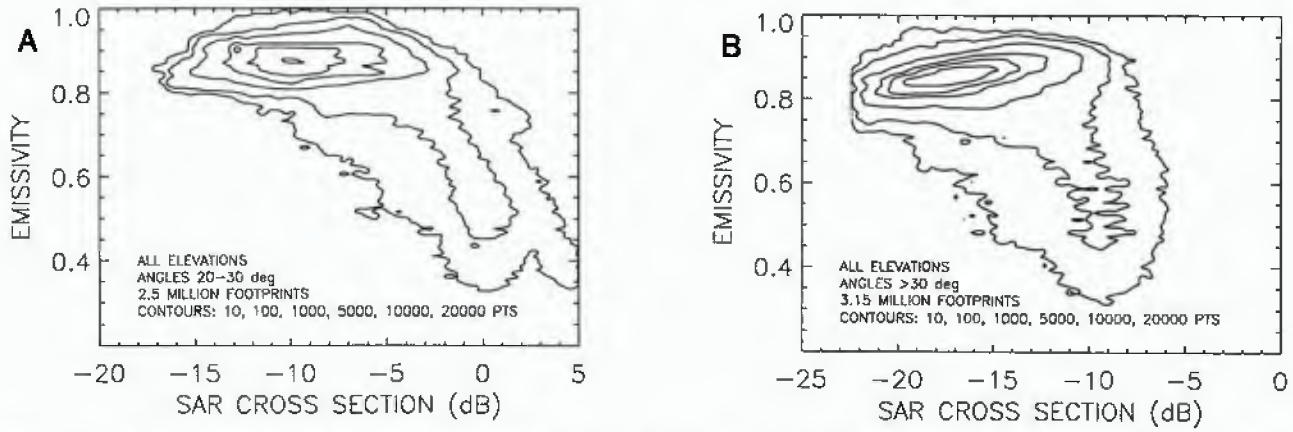

FIG. 4. Contour plots of H-polarized emissivity versus HH radar backscatter cross section. Data evaluated in 60 bins for σ_0 (−25 to 0 dB) and 100 bins for E (0.2 to 1.0). (A) All elevations, incidence/emission angle between 20° and 30°; (B) all elevations, angles >30°.

A MODEL FOR SCATTERING AND EMISSION

If we assume that the linear portions of the $E(\log \sigma_0)$ graphs for H polarization represent the behavior of a surface at a single average dielectric constant but with varying roughness, then the emissivities at the extreme ends of the linear portion should correspond to the dielectric constant of a smooth and a rough surface at the chosen incidence angle. For the graphs in Fig. 6B, we can fit both ends of each plot with a dielectric constant of 4.0–4.5 (Table I). If the high end of the V-polarized graph in Fig. 7B represents a specular surface, then the dielectric constant would fall between 3.76 and 4.38 (Eq. (3)) for the first five data points (based on the average incidence angle of footprints contributing to each point). We can also derive a best-fit linear function to the $E_h(\log \sigma_0)$ graph,

$$E = a \log_{10} \sigma_0 + b, \tag{5}$$

where a and b are the slope and intercept of the best-fit line. We have chosen to use a single average line for all data at angles >30°, since their best-fit lines were very similar up to −10 dB (Fig. 6). This similarity occurs because both parameters tend to decrease with angle (Figs. 1 and 2), and it appears that the behavior of the global mean surface is to simply shift values along a single line toward lower values of ε and E with greater angles.

The next step is to define the expected change in emissivity and backscatter cross section with variations in the dielectric constant. Based on the analysis of AIRSAR data for lava flows, we will assume that the change in cross section can be approximated by a multiplicative offset proportional to the change in Fresnel reflectivity at normal incidence (Campbell *et al.* 1993). The emissivity change depends on the incidence angle and the percentage of the surface which is rough. In this model, the surface is assumed to be composed of a mixture of perfectly rough and perfectly smooth terrain, which permits a continuum

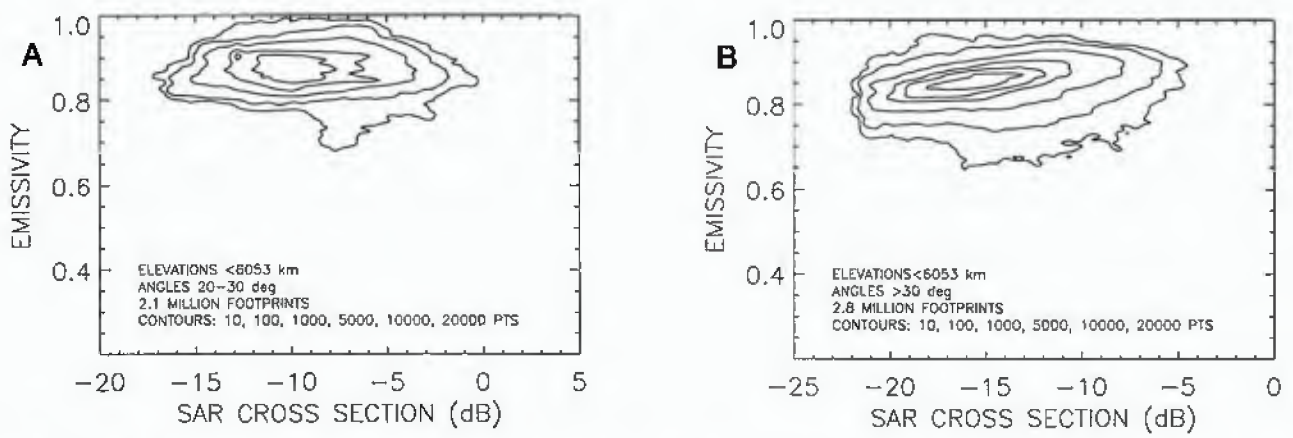

FIG. 5. Contour plots of H-polarized emissivity versus HH radar backscatter cross section. Data evaluated in 60 bins for σ_0 (−25 to 0 dB) and 100 bins for E (0.2 to 1.0). (A) Elevations <6053.0 km, incidence/emission angle between 20° and 30°; (B) elevations < 6053.0 km, angles >30°.

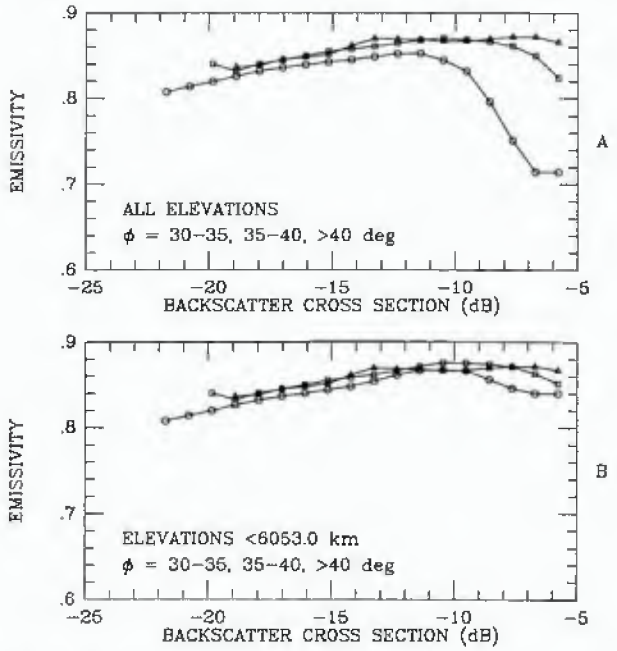

FIG. 6. Plots of average emissivity versus backscatter cross section (in dB) for three bins of incidence angle (triangles = 30°–35°, squares = 35°–40°, circles = >40°). (A) All elevations, (B) elevations <6053.0 km. Note the linear relationship between E and $\log(\sigma_0)$ for lowland areas.

of roughness; a similar assumption is made in correcting the Hagfors reflectivity derived from altimeter echo modeling (Pettengill *et al.* 1988),

$$\sigma_0^* = \sigma_0 \frac{R_0^*}{R_0} \tag{6}$$

$$E^* = fT_h^* + \frac{(1-f)(T_h^* + T_v^*)}{2}, \tag{7}$$

where σ_0^* and E^* are the observed SAR cross section and emissivity, f is the fraction of surface which is smooth, σ_0 is the SAR cross section of the surface at the mean dielectric constant ε, R_0 is the normal reflectivity at ε, and T_h^*, T_v^*, and R_0^* are the transmission and reflection coefficients (Eqs. (1–4)) evaluated at the actual surface dielectric constant ε^*. In order to solve this pair of equations for the dielectric constant ε^* and the smooth surface fraction f, we require a functional relationship between σ_0 and E for a known dielectric constant. This is provided by the global average behavior found above.

If we rearrange Eq. (7) above to solve for f we obtain

$$f = \frac{2E^* - (T_h^* + T_v^*)}{(T_h^* - T_v^*)} \tag{8}$$

and can then substitute Eq. (5) into this expression to solve for the smooth-surface fraction of points along our global average graph,

$$f = \frac{2a}{(T_h - T_v)} \log_{10}\sigma_0 + \frac{(2b - T_h - T_v)}{(T_h - T_v)}, \tag{9}$$

where in this case the transmission coefficients are evaluated at the mean surface dielectric constant ε. Solving Eq. (9) for σ_0 we obtain

$$\sigma_0 = 10^{\wedge}\left[\frac{(T_h - T_v)}{2a}\left(f - \frac{(2b - T_h - T_v)}{(T_h - T_v)}\right)\right]. \tag{10}$$

Finally, we substitute this expression and Eq. (8) into Eq. (6) to derive

$$\sigma_0^* = \frac{R_0^*}{R_0} 10^{\wedge}\left[\frac{(T_h - T_v)}{2a}\left(\frac{2E^* - (T_h^* + T_v^*)}{(T_h^* - T_v^*)} - \frac{(2b - T_h - T_v)}{(T_h - T_v)}\right)\right]. \tag{11}$$

This equation represents the solution to the model, as it relates the observed backscatter and emissivity, incidence angle, and mean dielectric constant to the correct surface dielectric constant (which appears in the asterisked transmission and reflection coefficients). Unfortunately, there is no way to solve this equation directly for the dielectric constant ε^*, so we must obtain a solution iteratively for each footprint. Once the dielectric constant is determined, the value for f (the smooth-surface fraction) comes from Eq. (8). In mapping the roughness, we use the value $(1-f)$ to show rougher areas as bright.

The results of this model can be plotted as a solution field. Figure 8 shows such fields for values of the incident/emitted angle of 30° and 45° (spanning the range of the

TABLE I
Values of Linear Least-Squares Fit to Data for Emissivity Versus Log(σ_0) Shown in Fig. 6b

Angular range	Slope	Intercept	Smooth-Surface E, ε	Rough-Surface E, ε
30–35°	0.044	0.919	0.836, 4.26	0.870, 4.46
35–40°	0.044	0.921	0.832, 3.97	0.876, 4.22
40–45°	0.054	0.926	0.808, 4.02	0.867, 4.37

Note. Regression performed only on portion of graph from −22 to −10 dB. Also shown are values of the emissivity (E) and estimates of the dielectric constant for the minimum backscatter cross sections on each line (assuming these are smooth surfaces) and at a cross section of −10 dB (assuming these are rough surfaces).

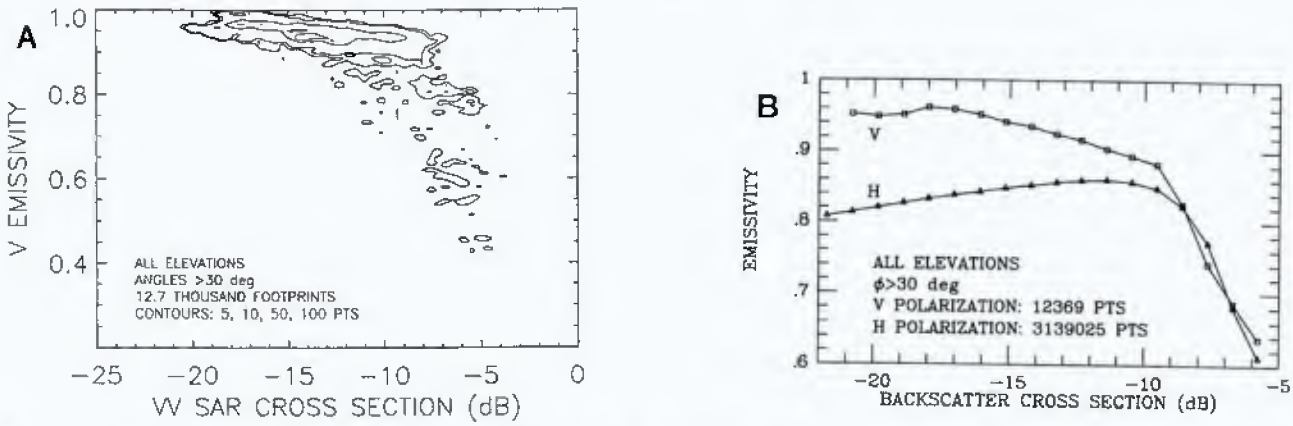

FIG. 7. (A) Contour plot of E versus σ_0 for V-polarized emissivity and VV radar backscatter (incidence angles >30°, all elevations). (B) Average H- and V-polarized emissivity versus backscatter cross section. H-polarized data represent an average over the entire planet (34°S–54°N), while V data come from 11 orbits in which the spacecraft was rotated about its axis. Note the convergence of the two plots at values of σ_0 of −9 dB.

model's applicability). Lines of constant dielectric constant (2, 4, 6, 8, 20, 50) and rough-surface fraction (0, 20, 40, 60, 80, 100%) are plotted. Note the increasing degree of compression in the model's range with decreasing incidence angle, as expected from the plots in Figs. 1 and 2. Relative to these plots, the a'a/pahoehoe threshold of −9 to −10 dB used in Campbell and Campbell (1992) requires surface roughness at the 80–100% level.

EFFECTS OF MIXED SURFACES

In this section we discuss the effect of applying the model to surfaces which are comprised of two or more distinct dielectric components (such as rock and soil). The major assumption required in using this model is that the linear relation between emissivity and $\log(\sigma_0)$ can be attributed to roughness variations imposed on a surface with some mean dielectric constant. This approach assumes that changes in bulk chemistry or density are not preferentially associated with any particular surface roughness. Variations in these properties would tend to cancel out when large areas are averaged, leaving only the more consistent behavior of E and σ_0 with roughness. It is possible that Venus is characterized by a regolith which varies in depth over the planet about some average value, in which case the mean ε found here represents a combination of the rock and soil components. The lack of extensive eolian features (Greeley *et al.* 1992) suggests that such a global regolith is at best shallow and coarse, formed by the weathering of local rock.

While their presence may not affect the global average microwave properties, there are likely surfaces composed of rocks lying on a background of fine soil (e.g., the Venera 13 site) or partially buried by crater ejecta or pyroclastic debris. The soil should appear primarily in the smooth-surface component of Eq. (7). The backscatter cross section will not vary dramatically as the dielectric constant of this soil changes, since the echo comes predominantly from the exposed rocky elements. The model will interpret a region with low smooth-surface dielectric constant to have a value of ε between that of the rock and the soil and will infer a roughness that is higher than that actually present. Likewise, a site with high-ε soil will have lower

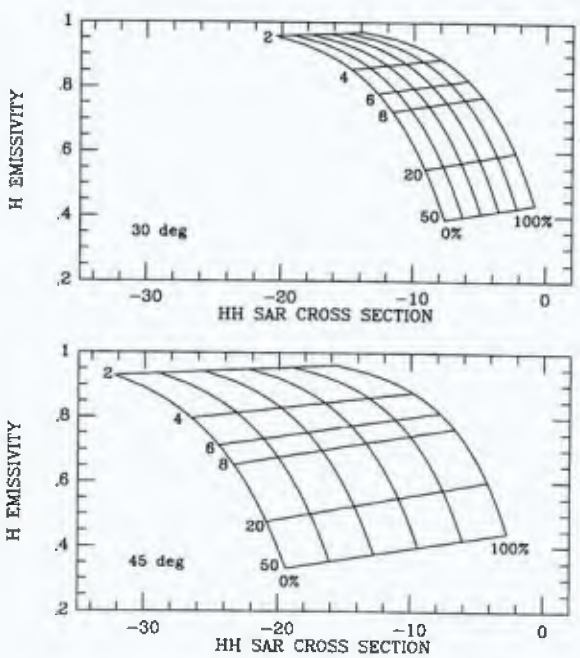

FIG. 8. Solution fields for the dielectric/roughness model. Lines of constant roughness fraction (0, 20, 40, 60, 80, and 100%) and constant dielectric constant (2, 4, 6, 8, 20, 50) are shown. (Top) Incidence/emission angle 30°. (Bottom) Incidence/emission angle 45°.

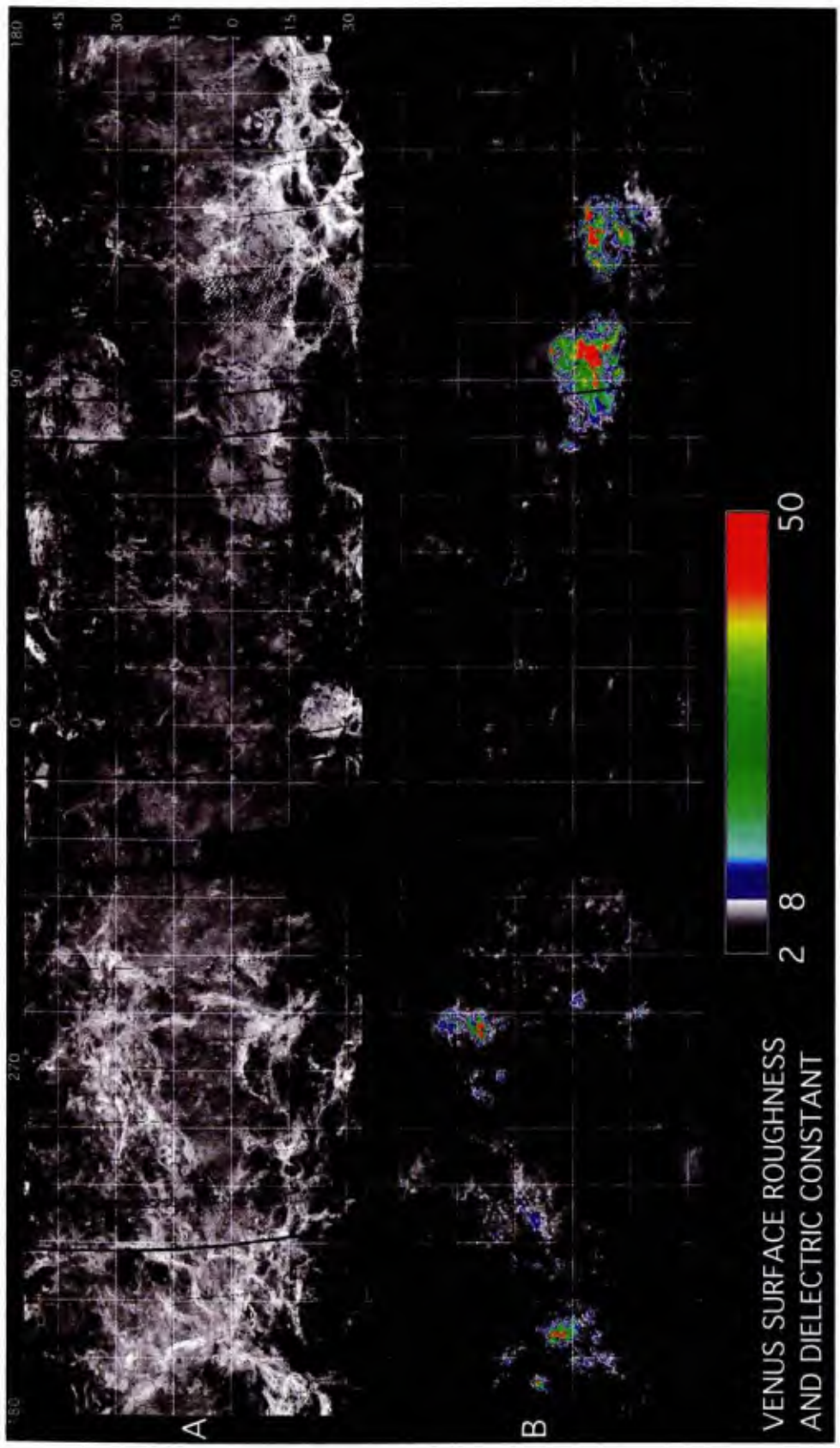

FIG. 9. Model results for region 34°S–54°N. Data resolution ~5 km along the orbit tracks, with most interorbit gaps filled in by a weighted 15 × 15-km boxcar filter. Cylindrical projection, with center longitude of 0° and grid spacing of 15°. (A) Roughness fraction (black = 0%, white = 100%). (B) Model-derived dielectric constant (color bar shown on image). Black areas are missing data.

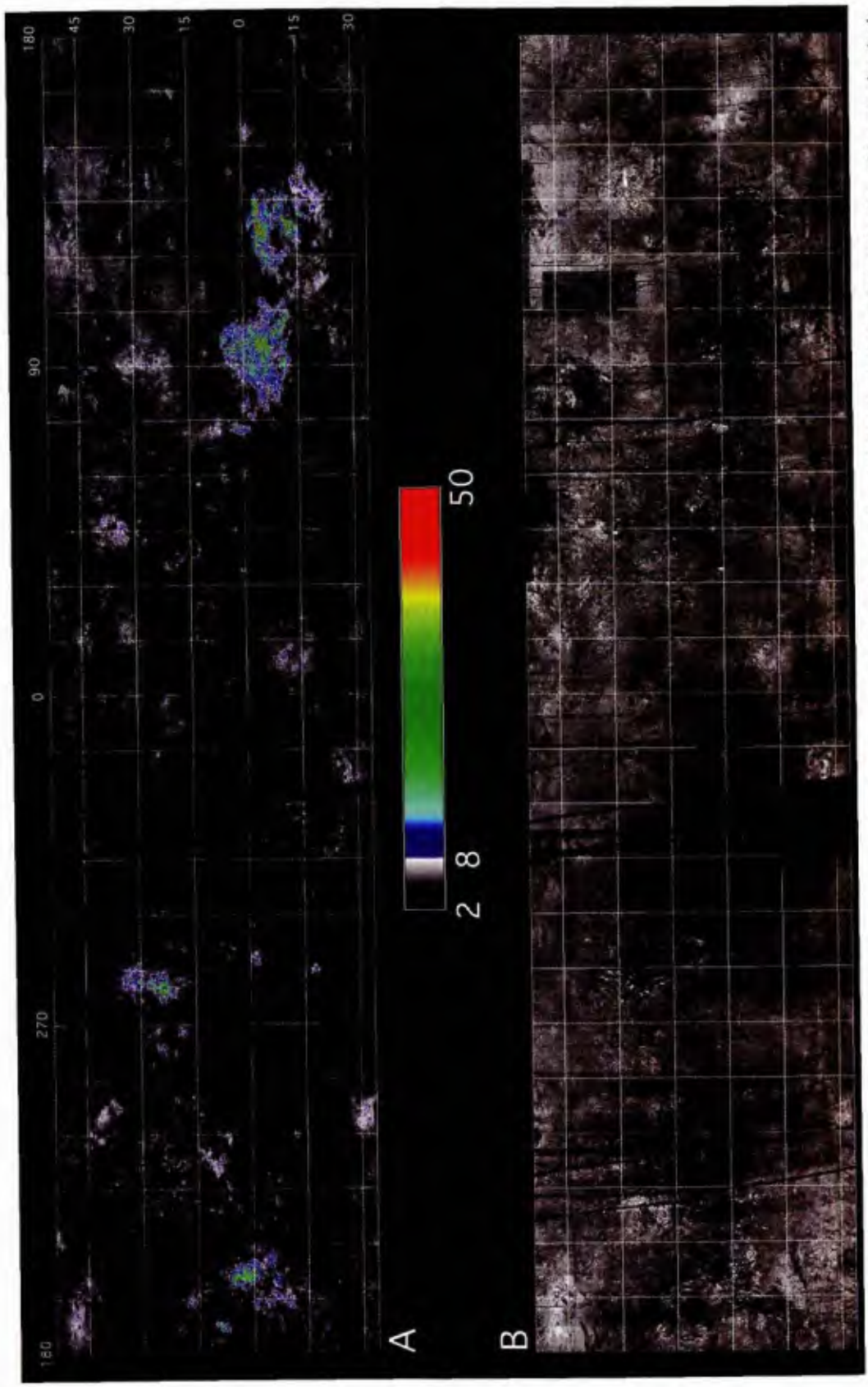

FIG. 11. (A) Image of Hagfors-model derived dielectric constant, based on corrected Magellan altimeter data (GREDR files). Cylindrical projection, with center longitude of 0° and grid spacing of 15°. Color stretch identical to that used in Fig. 9. (B) Ratio of dielectric constant from corrected reflectivity dataset to that derived from emissivity model (b = 0.25, w = 1.75). Note the generally good agreement between the two methods over the smooth plains and the very poor correlation in the radar-bright highlands.

model-derived roughness. The sense of the dielectric constant is thus correct for a mixed-ε surface (it will reflect a weighted average of the terrain within the cell), but the derived roughness may be incorrect. Obviously, the problem is worst for surfaces where the rock and covering material are evenly distributed over the footprint, since at zero and 100% soil coverage the model assumptions are again appropriate.

There are situations where this model will return a physically unreasonable value for the smooth-surface fraction ($f < 0$). This will occur in areas with significant radar-facing slopes, which enhance the backscatter return without any requisite rise in the dielectric constant or the wavelength-scale roughness. Strong quasi-specular echoes from certain surfaces (such as a rolling lava flow viewed at angles of 30° or less) could also lead to negative estimates of f. Values of f greater than unity could occur if the surface were tilted to an incidence angle much greater than that assumed for the spherical target.

MODEL RESULTS

The model described above was used to produce maps of roughness and dielectric constant for the area 34°S–54°N (Fig. 9; model parameters: $\varepsilon = 4.15$, $a = 0.05$, $b = 0.92$). The model parameters "a" and "b" were chosen based on the values shown in Table I. The mean dielectric constant of 4.15 was chosen from the center of the range of smooth-surface estimates in Table I. The original sparse images were smoothed using a 15 x 15-km weighted boxcar filter to fill in gaps between orbit tracks. Large gaps were left black. The model returns rough-surface estimates greater than 100% for radar-facing areas such as mountain belts or corona rims, but most footprints fall within the model's solution field at their respective viewing angles. This can be shown by overlaying solution graphs on the contour plots for the SAR and emissivity data in three angular bins (Fig. 10). The majority of high-reflectivity surfaces (those above 6053 km) fall within the 40–45° bin due to the clustering of highlands along the equatorial region.

The data in Fig. 10C suggest that high-dielectric surfaces tend to have higher roughnesses, with the mean behavior following the 80% rough-surface line. Is the application of the model to the highland areas valid? Although the model is derived from the linear trend seen in plots of E versus $\log(\sigma_0)$ for the lowlands, this does not rule out its utility in areas where changes in the dielectric constant may be equally as important as roughness variations. The validity of the basic relationships in Eqs. (6) and (7) determines the model's accuracy. If the high backscatter cross section and low emissivity in the highlands are the result of increases in the Fresnel reflectivity at the surface/atmosphere interface, then the model still generally holds (although multiple scattering may bias the results). If volume scattering within a radar-transparent material drives the low emissivity, then this model cannot be appropriate. Evidence from terrestrial radar data suggests that surface scattering (single and multiple events) could produce the observed highland circular polarization properties (Campbell *et al.* 1993), and the reasonable fit between the model and the "rollover" in plots of E versus $\log(\sigma_0)$ offers no reason to discard the single high-dielectric interface theory of Pettengill *et al.* (1988).

We can compare the results of this model to the Magellan corrected reflectivity data for Venus (Fig. 11A). Fresnel reflectivities were derived by fitting a Hagfors scattering function to the near-nadir echoes measured by the Magellan altimeter (Ford and Pettengill 1992). These values are typically lower than the true reflection coefficient due to diffuse scattering from the surface, which spreads the incident power over a large angular range (Bindschadler and Head 1988). A correction factor is introduced into the altimeter data reduction which uses the SAR backscatter intensity to estimate the fraction of rough terrain in a footprint and to thus normalize the Hagfors reflectivity (Pettengill *et al.* 1988). For very smooth surfaces the correction will be minor, but on rough terrain this factor is crucial to obtaining a correct estimate of the reflectivity. This correction technique will not work well in regions of rapidly varying roughness (i.e., tessera) where the returned echo selected by the altimeter echo-modeling algorithm may represent only a small portion of the terrain in the footprint. Additional corrections were needed to remove systematic variations in the Fresnel reflectivity with true anomaly.

The ratio of Hagfors-derived dielectric constant to that found with the emissivity model is shown in Fig. 11B. The model-derived dielectric constants are typically slightly higher than those from the Hagfors fit, but the general correlation between the two methods is good over smooth areas. In rough lava flows and tessera regions the Hagfors fit and subsequent SAR correction appear to undercompensate for the actual diffuse return, since the reflectivities for these areas are consistently lower than the emissivity model results would indicate. In bright highland regions the average Hagfors values fall well short of the emissivity-derived dielectric constants, perhaps due to errors introduced by the diffuse scattering correction at very high backscatter values.

GEOLOGIC RESULTS FOR SELECTED AREAS

In this section we examine the results of the dielectric constant model in the context of Venus geology and surface properties. The data compiled above and the model output reveal several major classes of behavior which are discussed separately below.

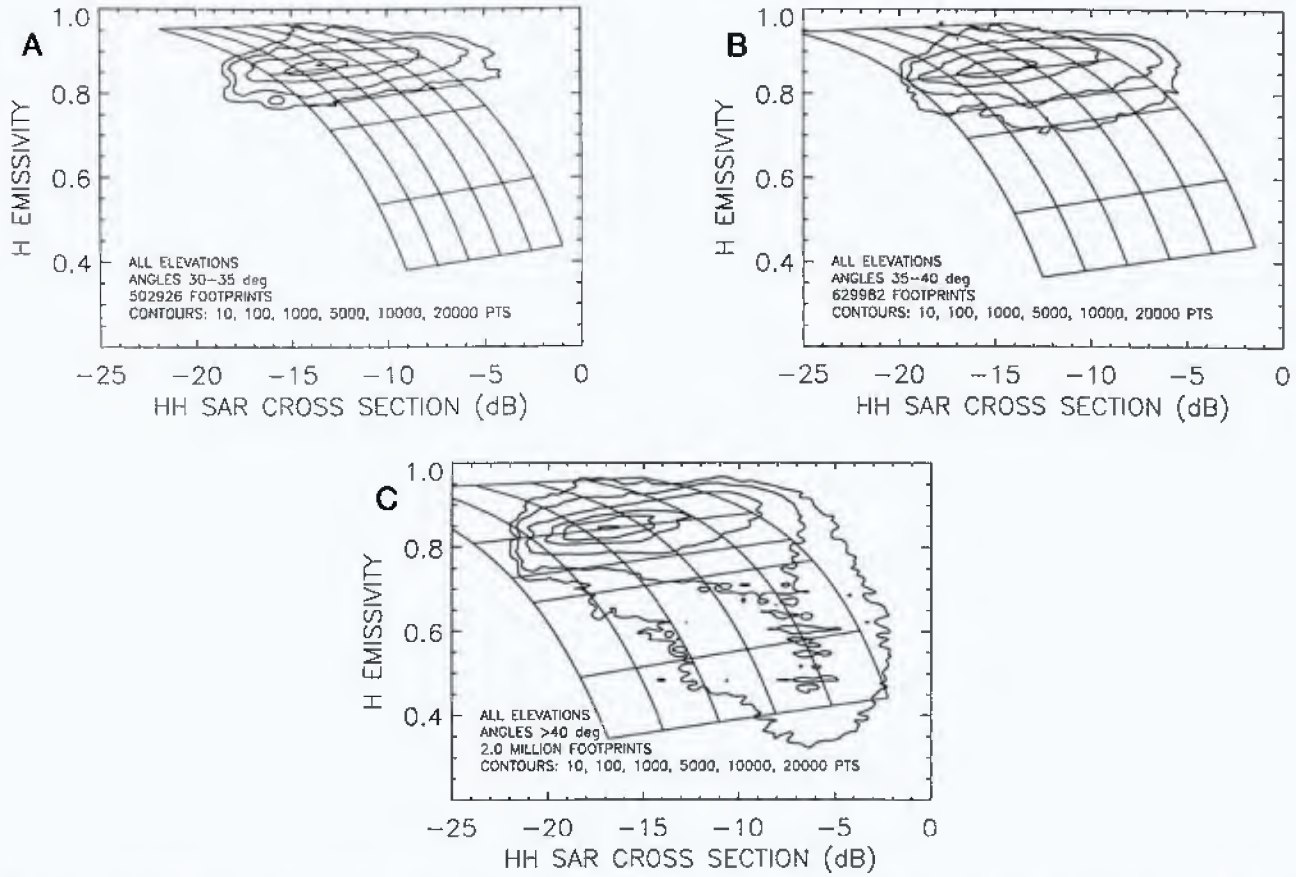

FIG. 10. Solution fields for the model overlayed on contour plots of emissivity versus radar backscatter cross section for three incidence angle bins. Lines of equal dielectric constant (2, 4, 6, 8, 20, 50) and roughness (0, 20, 40, 60, 80, and 100%) identical to those used in Fig. 8. The majority of high-dielectric points fall in the >40° angle bin due to the concentration of highlands along the equatorial belt. Note the tendency for higher dielectric areas to have roughness of ~80%. (A) Incidence/emission angle 30°–35°. (B) Incidence/emission angle 35°–40°. (C) Incidence/emission angle >40°.

Highlands

Dielectric values in the highlands within our study area (34°S–54°N) tend to rise with altitude to values of 50 or more. A value of $\varepsilon = 8$ is a good delimiter of highland and lowland dielectric constant ranges, as shown by Fig. 9. As discussed above, the model data are consistent with a single high-dielectric interface for these regions rather than an internal volume-scattering regime (Pettengill *et al.* 1992, Tryka and Mulheman 1992, Wilt 1992). There are instances of both smooth and rough high-dielectric surfaces, but the dominant trend is toward high roughness (80% or more) in areas with moderate-high values of ε. This may indicate that a physical weathering process occurs in conjunction with formation of high-permittivity mineral components.

Lava Flows

The lava flows which comprise the large edifice complexes vary in their dielectric properties. Values of ε from 3 to 9 are found in the lowlands, with dielectric boundaries often closely associated with specific flow units. The lava flows surrounding Sif Mons (21°N, 350°E) and the long bright flow north of Gula Mons (21°N, 359°E) have dielectric constant values of 5–7. Flows southeast of Maat Mons reach ε values of 9; the SAR, roughness, and dielectric constant data for this region are shown in Fig. 12. The large lava flow field south of Ishtar Terra (50°N, 345°E) has a very high roughness fraction and dielectric values close to 3, possibly due to superposed fine crater ejecta. The differences in dielectric properties between lava flows may be attributable to variations in vesicularity or, more likely, to differences in bulk chemistry (titanium or iron content) between batches of magma.

Robinson and Wood (1993) propose that low emissivity values found in the lowlands near some edifices (e.g., Maat Mons) are evidence for recent volcanic outgassing and conversion of basalt to more pyrite-rich forms. One example cited by these authors (their Fig. 5) does not appear to have enhanced dielectric values, and in fact

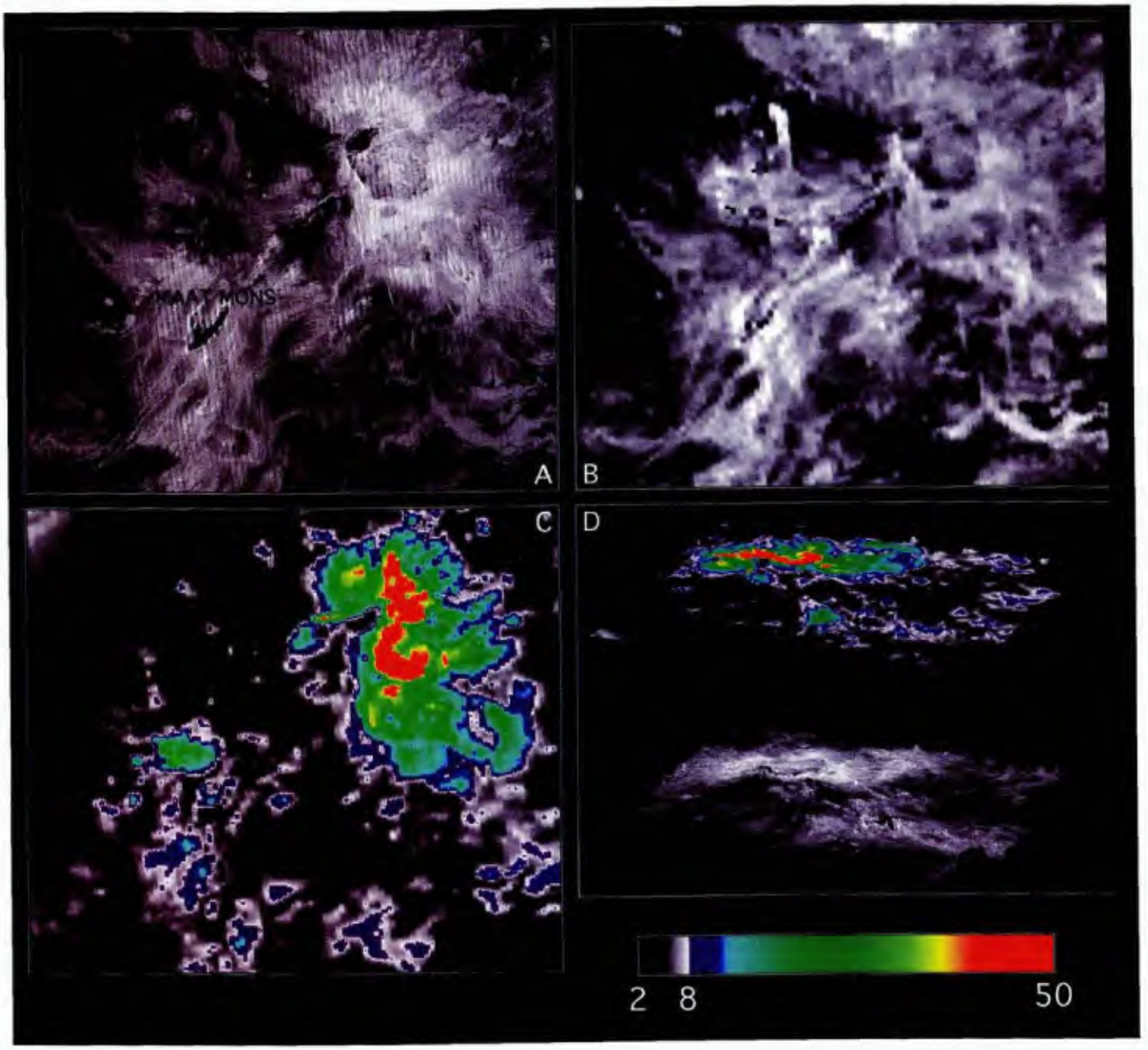

FIG. 12. Magellan data and model results for the area around Maat Mons (7.63°S–7.64°N, 188.5–206.2°E). (A) SAR image; black arrow points to low-ε area shown in Fig. 15. (B) Roughness map (b = 0%, w = 100%). The three clusters of black points on the flanks of Maat Mons represent footprints for which the model returned dielectric constant values <2. (C) Dielectric constant, with color stretch identical to that of Fig. 9B. (D) Perspective views of study area with SAR (top) and dielectric constant (bottom) overlayed on topography.

occurs in a large low-ε region. While there are high-dielectric lava flows near Maat Mons and at least one pitted dome of such material (Fig. 12), these features are more consistent with localized eruptions of magma with significant amounts of metallic minerals than with outgassing. The presence of moderate-ε material at the summit of Maat Mons is still open to interpretation, but there is little evidence to support the notion of "pyritization" in the lowlands around large volcanoes.

Crater Deposits

Many of the dielectric values >4 in the plains are related to impact craters. There are several high-dielectric crater

floors, of which Mead (12.5°N, 57.2°E) and Stuart (30.75°S, 20.2°E) are particularly good examples. Mead's floor is split between a typical plains permittivity on its western half and values around 8 in the eastern portion. Many of the crater parabola deposits have dielectric constant values of 6–7 (Campbell *et al.* 1992, Plaut and Arvidson 1992). There is a large parabola with ε of up to 7, related to the 13-km crater Miriam (36.5°N, 48°E), surrounding Nefertiti corona.

Crater parabolas are formed by airfall emplacement of fine-grained material during the late stages of the impact event, while bright floor material is likely impact melt (Campbell *et al.* 1992, Schultz 1992). If we assume that the high dielectric values are due to exposure of material with an intrinsically high permittivity, and not to any exotic scattering effect, then we need to explain why such material is routinely found in crater-related deposits. While dense basalt can have a dielectric constant of up to 9 (Ulaby *et al.* 1989), a mantling layer of impact ejecta is more likely to have permittivities consistent with rock powders (ε=2–3). In order to reach the dielectric constants observed here (6–8), the parabola-forming material must be "loaded" with conducting material (Pettengill *et al.* 1988, Shepard *et al.* 1994). Schultz (1992) has proposed that the parabolas are largely composed of impact melt, so perhaps the process of melting and recondensation serves to produce a loaded dielectric material. High-ε impact melt might also explain the radar-bright floors.

There are few areas where the parabolas can be seen well on the radar backscatter image, suggesting that they are quite thin. In this case (as discussed above), the high-dielectric mantling material does not cover a large amount of the rocks on the surface, so the emissivity declines with little change in the backscatter cross section. The model interprets this as a high-dielectric interface with low roughness. In such cases the roughness estimate must be treated with caution, but the dielectric value correctly reflects the average properties of the terrain.

There are also instances of low-dielectric deposits associated with impact craters. Northeast and east of Gula Mons there are two extensive low-ε areas (Fig. 13). The northeast region is centered on a probable impact feature (a radar-bright "V" shape within a radar-dark oval) along the north margin of the large lava flow field (Fig. 13D), while the second low-ε deposit is associated with the crater Annia Faustina (Campbell *et al.* 1992). The model results show a smooth region with ε~4 west of Faustina and values of 2–3 for the high-emissivity material related to the two impact features. Campbell *et al.* (1992) suggested that fine-grained, low-ε impact ejecta from Faustina crater mantles the eastern lava flows of Gula Mons (labeled in Fig. 13A). It appears from the model results that there are two features in this area which produced such mantling material and that these deposits have merged to create the large region of high emissivity. In this case, the dielectric values are correct, but the roughness results are likely too high because of the mixed terrain. The low-dielectric crater deposits may be mantling material which either never included a conductive phase, or in which this material has been weathered away by the atmosphere.

Possible Soil, Pyroclastic, or Ignimbrite Deposits

There are several instances of low-ε, variable roughness surfaces which do not have associated impact features. We discuss examples of these below and speculate on their possible modes of formation.

A triangular wedge of low (~2.5) dielectric constant material occurs just south of the Tepev Mons summit (Fig. 14). The SAR data show a low-return area which narrows downslope to the southwest, while the region of low permittivity widens downslope. Close examination of the SAR imagery suggests some sort of mantling deposit, but the apex of the triangle falls within a data gap. It is possible that this is an impact ejecta deposit whose parent crater is in the data gap or a "splotch" feature with no associated crater. A second possibility is that this is an unconsolidated volcanic deposit which has been spread downhill by the prevailing wind. Another deposit of this type occurs on the north flank of Maat Mons, where ε values drop to 2 over a three-lobed area downslope of a radar-dark dome (Fig. 12). In this case it appears that no nearby crater or splotch produced the material. In one area, mapped by Klose *et al.* (1992) as an "ash flow," the radar-bright lava complex appears to be mantled by fine debris (Fig. 15). Given the inhibition of volatile exsolution and pyroclastic volcanism on Venus (Garvin *et al.* 1982), an airfall origin for these units seems unlikely. One possibility is the emplacement of ignimbrite surge deposits, which may travel some distance along the ground in the dense atmosphere. This would be consistent with the downslope trend in the two deposits, which is not required of an airfall pyroclastic. Where the radar return is low we may assume that the fine material has covered many of the rocky scattering elements, while in areas with higher backscatter (but low ε) the debris layer must be quite thin.

Low ε values are found for several radar-dark lava flow patches near 30°S, 42°E (Fig. 16). These dark lava flows cover and embay portions of the tessera in this region, and are in turn cut by later graben and fractures. Radar-bright plains flows have embayed much of this older lava surface and infilled the graben. Given that these dark lava flows are stratigraphically quite old, the emissivity increase may be evidence for a possible soil layer or coverage by fine material from old impact craters. Low ε values also occur in clusters of elongate or dumbell-shaped fea-

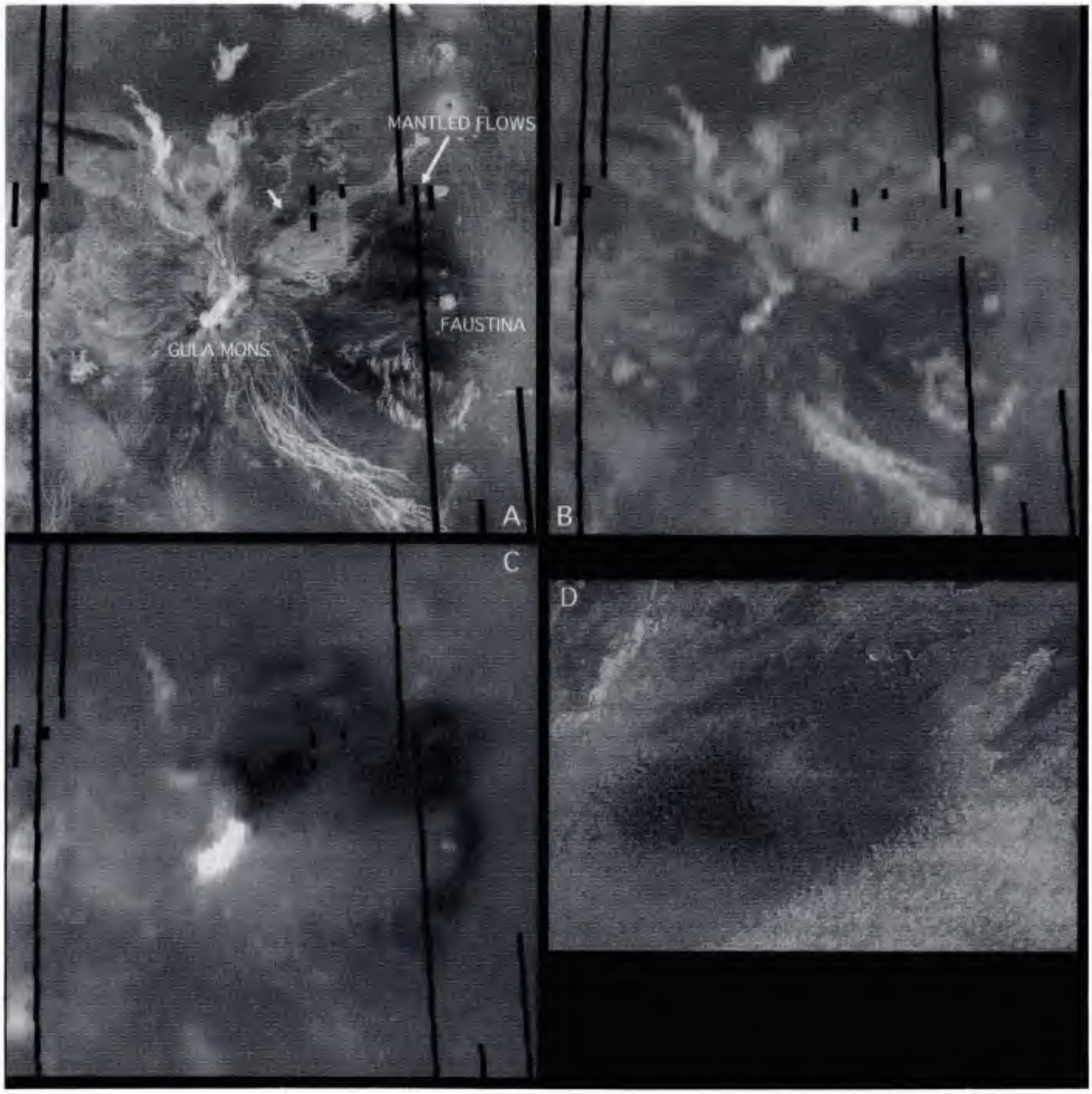

FIG. 13. Magellan data and model results for Gula Mons (16.5–29.5°N, 352.9–7.1°E). (A) SAR image; short white arrow indicates location of probable impact feature shown in Fig. 13D. (B) Roughness map (b = 0%, w = 100%). (C) Dielectric constant (b = 2.0, w = 8.0). (D) Magellan F-MIDR (75-m resolution) view of the oval dark deposit northeast of Gula Mons. Note the bright central region and associated east-pointing radial ejecta pattern. Image width 112 km, north at top.

tures, some of which parallel large topographic highs such as tesserae or ridge belts. The origin of these features is unclear; they do not appear to be crater-related and are associated with both radar-bright and radar-dark surfaces. These features may be areas of eolian accumulation (due to locally low topography) or older lava flows with a covering of unconsolidated material.

Venera Landing Sites

As an additional test of the model, we tabulated all of the radiometer footprints that fell within a 300-km box around the landing sites of Veneras 9, 10, 13, and 14 (Basilevsky *et al.* 1992, Weitz and Basilevsky 1993). We then calculated a mean dielectric constant and roughness

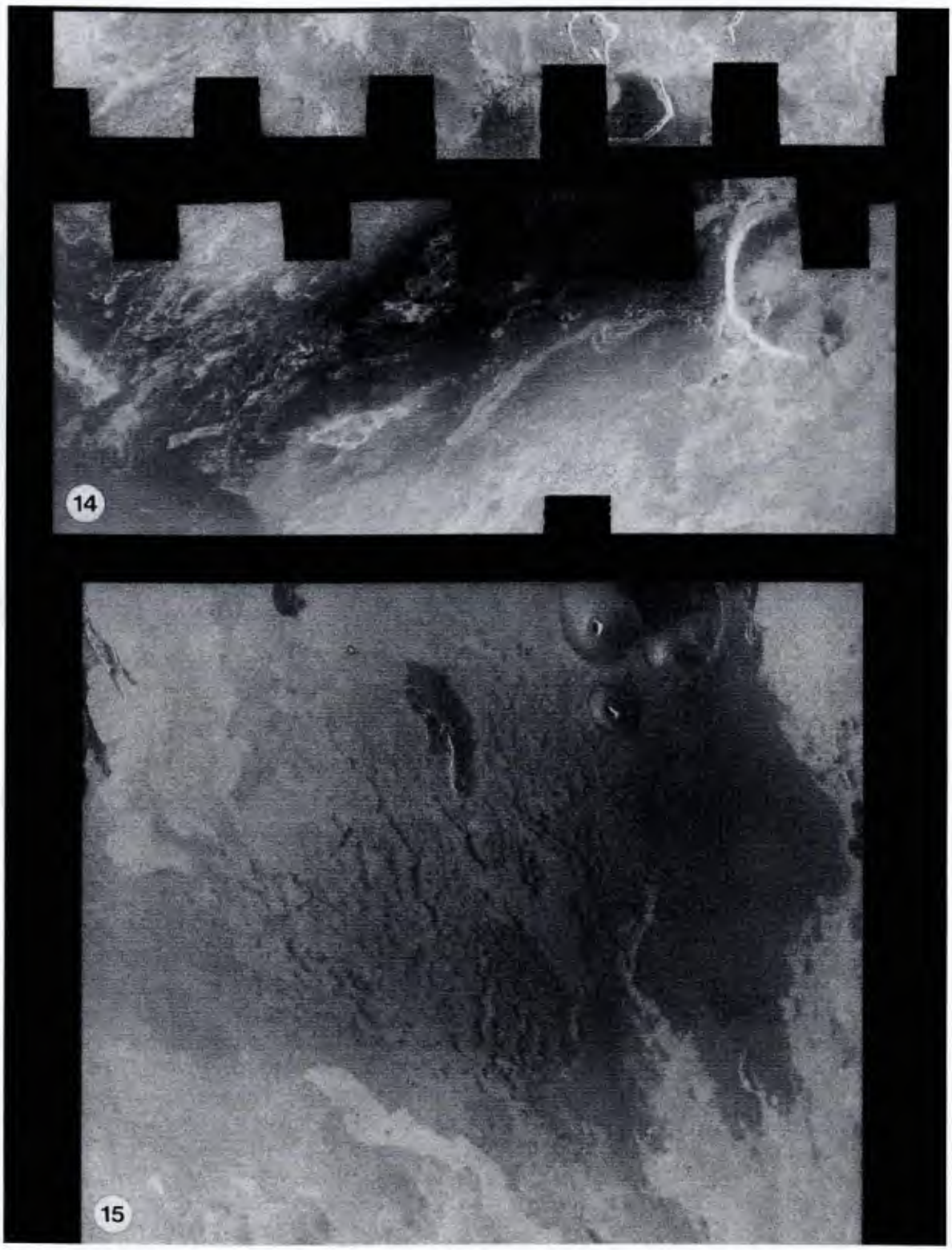

FIG. 14. Magellan radar image of low-ε, low-σ_0 wedge on Tepev Mons south flank (28.0–29.0°N, 44.0–46.0°E). Image height 105 km. The low radar return region narrows downhill to the southwest, suggesting a "source" within the data gaps northwest of the steep-sided dome.

FIG. 15. Magellan radar image of low-return area north of Maat Mons (2.0–3.5°N, 194.0–195.4°E). Image height 160 km. Note the subdued appearance of features within the rough lava flows in the center of the image, suggesting partial mantling by fine-grained material.

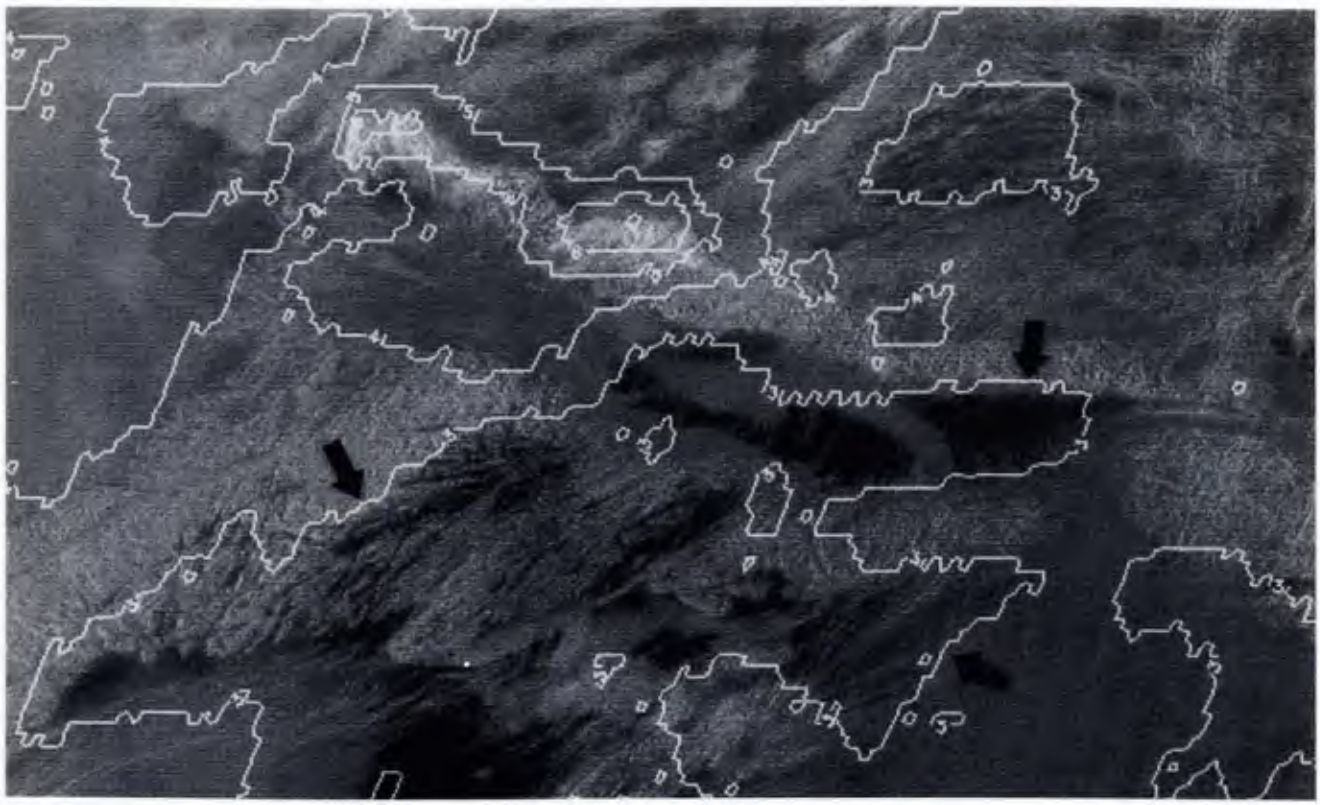

FIG. 16. Magellan radar image of plains and tessera units with contours of dielectric constant overlayed (30.5–34.0°S, 39.0–45.5°E). Contour values plotted for ε values of 2, 3, 4, 5, 6, 7, and 8. Note the low values of ε (3.0 contour marked by black arrows) associated with the radar-dark lava flows.

from the model solutions to these points. Table II presents the results of this analysis. In general, the four landing sites exhibit a narrow range of dielectric constant, from the Venera 9 value of 4.18 (close to the planetary average of 4.15 used in the model) to a value of 5.07 around the Venera 14 site. Only the Venera 9 site displays an obvious correlation between model results and the lander view (a rubbly surface with 80% roughness). The roughnesses derived for the other three sites (57–69%) do not correlate well with the lander views, although these panoramas represent very small regions within the 9×10^4 km^2 sample boxes.

TABLE II
Values of Model-Derived Roughness Fraction and Dielectric Constant for Four Venera Lander Sites

Lander	Footprints	Mean ε	Mean roughness fraction
V9 (31.01°N, 291.64°E)	678	4.18 ± .01	0.80 ± .004
V10 (15.42°N, 291.51°E)	1044	4.76 ± .01	0.69 ± .004
V13 (07.55°S, 303.69°E)	883	4.89 ± .01	0.57 ± .003
V14 (13.05°S, 310.19°E)	764	5.07 ± .01	0.64 ± .004

Note. Values for each site represent mean of all solutions within the 300-km box surrounding landing site estimate (Basilevsky *et al.* 1992).

CONCLUSIONS

Based on the observations of emissivity and radar backscatter across Venus, we proposed that many variations in emissivity for angles >30° can be explained by changes in surface roughness and presented a model which estimates the dielectric constant of the surface using a simplified treatment of scattering and emission. The model provides a rapid way of identifying areas of differing composition or density, but further work is required to understand the specific geology of each anomalous region. The combination of H- and V-polarized emissivity data for some surfaces will permit the use of two-component dielectric models (such as rock and soil with different values of ε). The type of analysis presented here, which integrates all available data for geologic studies, should improve the utility of the Magellan datasets for mapping and interpretation.

The permittivity in highland regions rises with altitude, and the data for these areas are more consistent with a single high-dielectric interface than with volume scattering. Higher dielectric constants are associated with both smooth and rough terrains, but the general tendency is toward greater roughness with higher permittivity. This may suggest that a mechanical weathering process occurs in the formation of high-dielectric mineral phases. There are variations in dielectric constant within lava flow complexes (up to values of 9), which may reflect differences in the chemical content of the rock. Three major types of mantling deposits are identified: (1) high-permittivity (ε = 7–8) units associated with parabolic crater features and interpreted to be fine-grained material with a high proportion of metallic phases; (2) low-permittivity (ε = 2–3) crater-related splotches or haloes, interpreted to be fine-grained material with minimal or weathered metallic minerals; (3) low-permittivity deposits with no associated crater, tentatively attributed to soil formation or to pyroclastic or ignimbrite eruptions. Within each type of deposit there is a range of surface roughness and radar backscatter strength, which are related to the original surface roughness and the depth of the mantling material.

ACKNOWLEDGMENTS

This work was supported in part by grants from NASA's Planetary Geology and Geophysics Program (NAGW-3360) and Venus Data Analysis Program (NAGW-3724). The author thanks P. Ford, T. Maxwell, R. Arvidson, M. Shepard, D. Campbell, and J. Zimbelman for helpful discussions and reviews. Two anonymous reviewers provided many useful comments.

REFERENCES

Arvidson, R. E., R. Greeley, M. C. Malin, R. S. Saunders, N. Izenberg, J. J. Plaut, E. R. Stofan, and M. K. Shepard 1992. Surface modification of Venus as inferred from Magellan observations of plains. *J. Geophys. Res.* **97**, 13303–13318.

Basilevsky, A. T., O. V. Nikolaeva, and C. M. Weitz 1992. Geology of the Venera 8 landing site region from Magellan data: Morphological and geochemical considerations. *J. Geophys. Res.* **97**, 16314–16336.

Bindschadler, D. L., and J. W. Head 1988. Diffuse scattering of radar on the surface of Venus: Origin and implications for the distribution of soils. *Earth Moon Planets* **42**, 133–150.

Burns, R. G., and D. W. Straub 1993. Venus mountain-top mineralogy: Misconceptions about pyrite as the high radar-reflecting phase. *Lunar Planet. Sci. Conf. XXIV*, 233–234.

Campbell, B. A., R. E. Arvidson, and M. K. Shepard 1993. Radar polarization properties of volcanic and playa surfaces: Applications to terrestrial remote sensing and Venus data interpretation. *J. Geophys. Res.* **98**, 17099–17114.

Campbell, B. A., and D. B. Campbell 1992. Analysis of volcanic surface morphology on Venus from comparison of Arecibo, Magellan, and terrestrial airborne radar data. *J. Geophys. Res.* **97**, 16293–16314.

Campbell, D. B., N. J. S. Stacy, W. I. Newman, R. E. Arvidson, E. M. Jones, G. S. Musser, A. Y. Roper, and C. Schaller 1992. Magellan observations of extended impact crater related features on the surface of Venus. *J. Geophys. Res.* **97**, 16249–16278.

England, A. W. 1975. Thermal microwave emission from a scattering layer. *J. Geophys. Res.* **80**, 4484–4496.

Fegley, B., A. H. Trieman, and V. L. Sharpton 1992. Venus surface mineralogy: Observational and theoretical constraints. *Proc. Lunar Plan. Sci.* **22**, 3–19.

Ford, P. G., and G. H. Pettengill 1992. Venus topography and kilometer-scale slopes. *J. Geophys. Res.* **97**, 13102–13114.

Garvin, J. B., J. W. Head, and L. Wilson 1982. Magma vesiculation and pyroclastic volcanism on Venus. *Icarus*, **52**, 365–372.

Greeley, R., *et al.* 1992. Aeolian features on Venus: Preliminary Magellan results. *J. Geophys. Res.* **97**, 13319–13345.

Hagfors, T. 1970. Remote probing of the moon by infrared and microwave emissions and by radar. *Radio Sci.* **5**, 189–227.

Jurgens, R. F., M. A. Slade, L. Robinett, S. Brokl, G. S. Downs, C. Franck, G. A. Morris, K. H. Farazian, and F. P. Chan 1988. High resolution images of Venus from ground-based radar. *Geophys. Res. Lett.* **15**, 577–580.

Klose, K. B., J. A. Wood, and A. Hashimoto 1992. Mineral equilibria and the high radar reflectivity of Venus mountaintops. *J. Geophys. Res.* **97**, 16353–16370.

Pettengill, G. H., P. G. Ford, and B. D. Chapman 1988. Venus: Surface electromagnetic properties. *J. Geophys. Res.* **93**, 14881–14892.

Pettengill, G. H., P. G. Ford, and R. J. Wilt 1992. Venus surface radiothermal emission as observed by Magellan. *J. Geophys. Res.* **97**, 13091–13102.

Plaut, J. J., and R. E. Arvidson 1992. Comparison of Goldstone and Magellan radar data in the equatorial plains of Venus. *J. Geophys. Res.* **97**, 16279–16292.

Robinson, C. A., and J. A. Wood 1993. Recent volcanic activity on Venus: Evidence from radiothermal emissivity measurements. *Icarus* **102**, 26–39.

Saunders, R. S., *et al.* 1992. Magellan mission summary. *J. Geophys. Res.* **97**, 13067–13090.

Schultz, P. H. 1992. Atmospheric effects of ejecta emplacement and crater formation on Venus from Magellan. *J. Geophys. Res.* **97**, 16183–16248.

Shepard, M. K., R. E. Arvidson, R. A. Brackett, and B. Fegley 1994. A ferroelectric model for the low emissivity highlands on Venus. *Geophys. Res. Lett.* **21**, 469–472.

Stratton, J. A. 1947. *Electromagnetic Theory*. Wiley, New York.

Tryka, K. A., and D. O. Muhleman 1992. Reflection and emission properties on Venus: Alpha Regio. *J. Geophys. Res.* **97**, 13379–13394.

Ulaby, F. T., R. K. Moore, and A. K. Fung 1987. *Microwave Remote Sensing*. Addison-Wesley, Reading, MA.

Ulaby, F. T., T. Bengal, J. East, M. C. Dobson, J. Garvin, and D. Evans 1988. *Microwave Dielectric Spectrum of Rocks*, Rep. 23817-1-T. Univ. of Michigan Radiation Lab., Ann Arbor, MI.

Weitz, C. M., and A. T. Basilevsky 1993. Magellan observations of the Venera and Vega landing site regions. *J. Geophys. Res.* **98**, 17069–17098.

Wilt, R. J. 1992. *A Study of Areas of Low Radiothermal Emissivity on Venus*. Ph.D. dissertation, MIT.